Contrib. Plasma Phys. **44**, No. 7-8, 582 – 588 (2004) / **DOI** 10.1002/ctpp.200410085

Numerical Models of the Planar Magnetron Glow Discharges

I. Kolev * and **A. Bogaerts**

Research Group PLASMANT, Dept. of Chemistry, Univ. of Antwerp, Universiteitsplein 1, 2610-Wilrijk, Belgium

Received 15 April 2004, accepted 15 April 2004
Published online 29 October 2004

Key words DC Magnetron, PIC/MC, Numerical Simulation, Hybrid Model.
PACS 52.65.Pp, 52.65.Rr, 52.65.Ww, 51.60.+a

The outlines of two methods for numerical simulation - hybrid and PIC/MCC of DC magnetrons are presented. Typical results from both of them are shown and compared. The hybrid model is faster, but has limited validity range. The PIC/MCC model, on the other hand, is stable for all operational conditions and does not require any assumptions, but is computationally expensive.

1 Introduction

DC magnetron sputtering systems have been widely used for many years for deposition of thin films in material processing. They offer two main advantages. Firstly, the ease with which one can enlarge the deposition area due to the good plasma uniformity. Secondly, the deposition rate is higher in comparison to that obtained by using rf sputtering systems. It comes as a result of the possibility to sustain the magnetron discharges at low pressures in the range of few mtorr, which reduces the diffusion of the sputtered atoms back to the target. However, magnetron systems posses a strong disadvantage, namely, the low utilization rate of the target material. This is caused by the appearance of the so-called racetrack - localized target erosion due to the strongly non-uniform magnetic field at the cathode. The film quality, however, is much sensitive to the particle influence from the plasma. Thus, it is important to control the magnetron discharge structure not only in the vicinity of the cathode, but also before the substrate. A powerful tool for achieving this goal is the numerical modeling. For adequate results to be obtained, the model must be self-consistent and to account for the entire discharge with as less as possible assumptions and simplifications.

A number of models of magnetron discharges have been reported throughout the past decade. This includes fluid non self-consistent description of the cathode area [1], semi analytical one-dimensional model of low-pressure magnetron [2], pre-sheath model [3], semi-analytic description of a steady-state 1D magnetron [4]. Parallel to this, much work has been done in direct Monte-Carlo simulations of the cathode region. These are non self-consistent models, where the trajectories of the electrons are traced under various assumptions about the structure of the electric field - from simple linear dependence to some semi analytical relations taken from experiments. These simulations give satisfactory prediction of the erosion profile. But through such an approach it is impossible to determine the spatial density and energy distribution of the charged particles and the spatial potential. A detailed 1D self-consistent PIC/MCC study of a cylindrical post-magnetron was performed by van der Straaten et al. [5]. Appearance of negative apace charge mode was shown at low pressures and high magnetic fields. Nanbu et al. [6] performed the first 3D PIC/MC magnetron simulation. For the case of axisymmetrical magnets they proved [7] that the whole discharge is also axisymmetrical and so, could be correctly modeled in 2D cylindrical geometry (r,z). Even in 2D, however, the computational time is significant. This makes it desirable other than particle model to be used. The low pressure, normally used in magnetrons - around 5 mtorr, makes the

* Corresponding author: email: ivan.kolev@ua.ac.be, Phone: +00 32 3 820 2382, Fax: +00 32 3 820 2376

fluid description not necessarily valid. An alternative is a hybrid model - Monte Carlo/Fluid, which can account for the two electron groups - beamlike highly energetic electrons ejected from the cathode and the slow bulk electrons in the plasma. This approach was reported by Shidoji et al. [8]. Transport coefficients of the electrons in their work were obtained from a solution of Boltzmann equation for a set of **B**/n and **E**/n values, performed by Ness and Makabe [9].

In this work the outlines of the hybrid and PIC/MCC techniques will be given as used in the authors codes and some typical results will be shown.

2 Hybrid Model

In the hybrid model all plasma species are split into two groups - high-energy group with particle energies higher than $\mathbf{E}_{\rm thr}$ and low-energy group with particle energies less than $\mathbf{E}_{\rm thr}$. $\mathbf{E}_{\rm thr}$ is normally the threshold energy for the lowest energetic interaction of consideration. In the case of argon discharge it will be the excitation threshold energy.

2.1 Fast electrons

The fast electrons are treated as individual particles due to the restrictions arising from their highly non-equilibrium state. Their trajectories are traced from the moment an electron is created until it disappears. The later could be due to transfer to the slow (bulk) electron group or absorption from the electrodes. In this study, the background gas is Argon and the energetic border, which determines the belonging of the electrons to one of the aforementioned groups, is set to 8 eV. For each electron the Newton equation of motion with a Lorentz force term is solved in every time step:

$$\mathbf{F} = \mathbf{F}_{elec.} + \mathbf{F}_{magn} = q\mathbf{E} + q(\mathbf{v} \times \mathbf{B}) \tag{1}$$

where q stands for the electron charge, $\mathbf{E}$ and $\mathbf{B}$ are electric and magnetic fields and v is the electron velocity. The electric field is taken as an input from the fluid code, and the magnetic field is adopted from [10]. The equation of motion is solved numerically using the leapfrog scheme [11],

$$m\frac{\mathbf{v}_{new} - \mathbf{v}_{old}}{\Delta t} = \mathbf{F}_{old}; \qquad \frac{\mathbf{x}_{new} - \mathbf{x}_{old}}{\Delta t} = \mathbf{v}_{new} \tag{2}$$

which is of second order of accuracy and is time-centered. This gives to the code stability at larger values of the time step Δt. Collisions between electrons and neutrals are treated with Monte Carlo technique [12]. The probability and the type of collision (if any) are determined at the middle of each time step (to preserve time-centering) using a single random number [13], which is compared to the normalized probability P_k of the k-th collisional event.

$$P_k(\epsilon) = N_{Ar}\sigma_k(\epsilon)\sqrt{\frac{2\epsilon}{m_{e-}}}\Delta t \tag{3}$$

Here N_{Ar} is the density of the Ar atoms, σ_k is the cross-section for the k-th event, m_e is the mass of the electron and ϵ is its energy. In case of collision, new, post-collision, velocity is calculated using random numbers [14]. The deflection angle in all types of scattering is [15]:

$$\chi = arccos\left(1 - 2\frac{R}{1 + 8\epsilon(1 - R)}\right) \tag{4}$$

where R is a uniformly distributed random number in the interval [0,1], $\epsilon = E_e/E_0$, E_e is the energy of the incident electron and E_0 is Bohr energy. The collisions taken into account are elastic scattering, ionization and

excitation from the ground state. The electrons created during ionization are also traced. The code ends when all electrons - those started from the cathode and those created in ionizations have been followed. Normally 5000 cathode electrons were used. The results of the MC code are the ionization rate, the rate of creation of slow electrons and the fast electrons density. They are source terms in the mass balance equations for the ions and slow electrons and in Poisson's equation respectively. The so calculated rates are made physically dimensional using the cathode current. It could be a measured value from experiment.

2.2 Bulk electrons and ions

Bulk electrons and ions are described by the fluid model. An important assumption is that ion gyro radii are considered much larger than characteristic dimensions of the system. This is not a severe restriction, since the strength of **B** does not exceed 300 G in most of the sputtering systems. Thus, ions do not feel the magnetic field and in the drift-diffusion approximation of the Boltzmann equation their flux is given by:

$$\Gamma_r^{Ar^+} = \left(\mu^{Ar^+} n^{Ar^+} E_r - D^{Ar^+} \frac{\partial n^{Ar^+}}{\partial r}\right); \qquad \Gamma_z^{Ar^+} = \left(\mu^{Ar^+} n^{Ar^+} E_z - D^{Ar^+} \frac{\partial n^{Ar^+}}{\partial z}\right); \tag{5}$$

where μ and D are the mobility and the diffusion coefficients and n is the ion density. Electrons, with their small gyro radius, are highly restricted in their movement by the magnetic field. In fact, they are trapped along lines of the magnetic field and can travel in transverse direction only due to collisions. Their flux is given by:

$$\Gamma_r^{e^-} = -\frac{\mu_{\mathbf{B}=0}^{e^-}}{1+\frac{\omega_z^2}{\nu^2}} n^{e^-} E_r - \frac{D_{B=0}^{e^-}}{1+\frac{\omega_z^2}{\nu^2}} \frac{\partial n^{e^-}}{\partial r}; \qquad \Gamma_z^{e^-} = -\frac{\mu_{\mathbf{B}=0}^{e^-}}{1+\frac{\omega_r^2}{\nu^2}} n^{e^-} E_z - \frac{D_{B=0}^{e^-}}{1+\frac{\omega_r^2}{\nu^2}} \frac{\partial n^{e^-}}{\partial z}, \tag{6}$$

where ν and ω are the mean collision frequency and the gyro frequency and μ and D are the mobility and diffusion of electrons in the absence of magnetic field. Eq. 6 is derived under the assumption for crossed electric and magnetic fields, such that: $\mathbf{E} = (E_r, 0, E_z)$ and $\mathbf{B} = (B_r, 0, B_z)$ and is correct, strictly speaking, only for constant $\mathbf{B}$ parallel to $\mathbf{E}$. (z-axis is taken in the direction between electrodes.) It is quite reasonable in cylindrical magnetrons, whilst in plane magnetrons there are always gradients in all directions due to the curvatures of the magnetic lines and $\mathbf{B}$ is never 1D. In spite of that, reasonable results could be obtained even for plane magnetrons with the abovementioned assumptions. This effectively gives the flux expressions the same shape as in the non-magnetized case, but with modified transport coefficients. For both species the continuity equation is fulfilled:

$$\frac{\partial n^{e-,Ar+}}{\partial t} + div\Gamma^{e-,Ar+} = R^{e-,Ar+} \tag{7}$$

where R is the net rate of creation of electrons or ions. The electrical field is obtained from the Poisson's equation:

$$\Delta V = -\frac{q}{\epsilon_0}(n^{Ar+} - n_{fast}^{e-} - n_{slow}^{e-}) \tag{8}$$

where V is the electrical potential and ϵ_0 is the electrical permittivity of the vacuum. n_{fast}^{e-} and R are taken as input from the Monte Carlo code. Equations (5 - 8) form a closed system of equations towards the unknowns: n^{e-}, n^{Ar+} and V. Once V is known $\mathbf{E}$ is calculated from: $\mathbf{E}$ = - grad$V$.

2.3 Numerical procedure

The program starts with the Monte Carlo code. For the first run a guess is needed for $\mathbf{E}$. That could be the values from some previous run with similar conditions or any arbitrary, but yet, still physically reasonable profile. However, the closer to the real is the guess, the faster is the convergence. The time step for MC code is normally around 10^{-12}s. Once the fast electron density and the creation rates for the bulk electrons and ions are known the

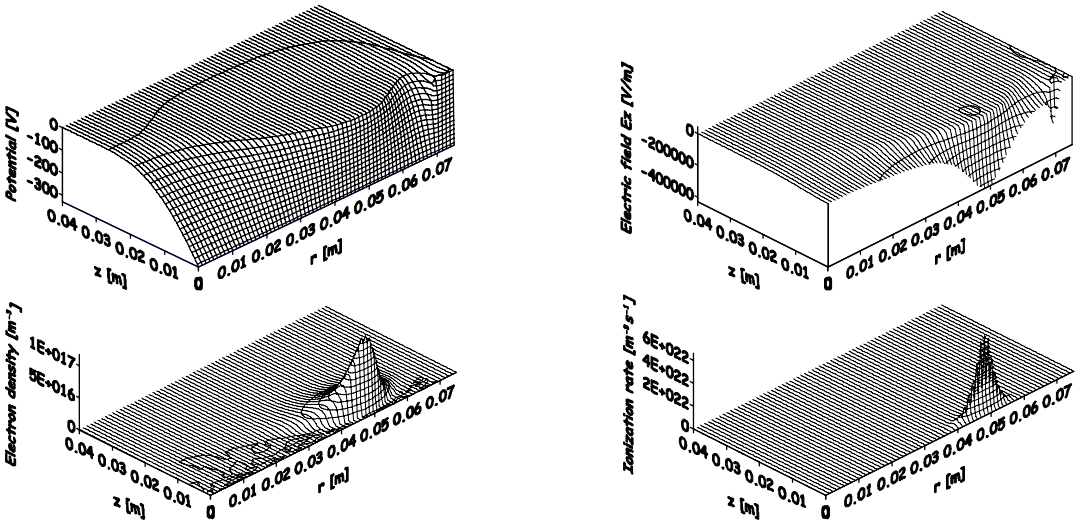

Fig. 1 Potential (upper left), axial electric field E_z (upper right), electron density (down left) and ionization rate (down right).

fluid code is executed to produce the slow electron and ion density distribution, electric field profile and ion flux at the cathode. The latest two are given back as input to the Monte Carlo code and the whole procedure is repeated until a steady state is obtained. Afterwards, the steady state fast electron energy distribution function (EEDF) is calculated. In the fluid code at each time step eqs. 6, 7 and 8 for the electrons are solved simultaneously. Due to the strong coupling and non-linearity they are solved using the so-called exponential scheme (Patankar [16]). Once $\mathbf{E}$ is known, eqs. 5 and 7 for the ions are solved using standard Thomas algorithm. The procedure is repeated until preset degree of accuracy is achieved. The results of the fluid code are electron and ions densities and fluxes, potential distribution and electric field distribution.

2.4 Results of the hybrid model

In this section we present some typical results from the model. All they are received under the following operating conditions: the voltage at the cathode is set to -330 V, $\mathbf{B}_{max}$ = 160 G, the anode is grounded, background gas pressure is 5 mTorr and the temperature is 300 K. Computational domain is a cylinder with dimensions r = 7.5 cm and z = 5cm. The gap between electrodes is equal to z, and the origin of the z-axis is at the cathode.

Showed results are in good agreement with the measured values taken from [10]. At stronger $\mathbf{B}$, however, the potential tends to more negative values very quickly and at $\mathbf{B} > 400$ G, becomes more negative than the cathode voltage. This is the well-known limitation of the classical diffusion across $\mathbf{B}$. We tried with Bohm diffusion coefficient, instead of classical, but the results were just slightly better (not showed here). The model can possibly be improved, if transport coefficients are taken not from the classical scaling, but from a swarm analysis. A better alternative, however, is to use a microscopic description, where the transport can be handled with no assumptions in a self-consistent manner.

3 Particle-in-Cell/Monte Carlo Collision Model (PIC/MCC)

The method in use is a standard PIC-MCC technique [11]. The charged particles - electrons and Ar^+ are replaced by superparticles. Their weight is the same and equal to 2.10^7. The superparticles move in the applied magnetic field and in an electric field, which is a superposition of the applied voltage on the electrodes and the field created by the superparticles themselves. Their movement and collisions are treated with the same procedure as that described above in the MC part of the hybrid code. The method is based on first principles only, hence no assumptions are needed. The procedure starts with an initial guess for the particle and velocity distribution - loading. Usually, velocity distribution at the beginning is considered Maxwellian. For the electrons a temperature of 1-2 eV is taken, while the ions are accepted to have room temperature. In the coordinate space, a

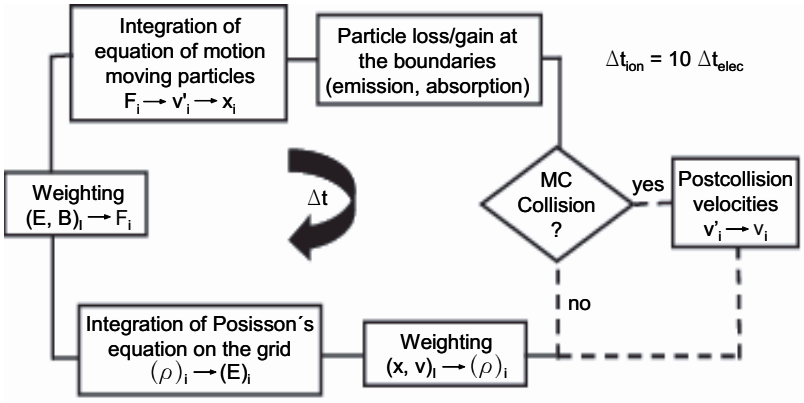

Fig. 2 Flow Chart of PIC/MCC simulation.

uniform distribution can be chosen, although it will make the convergence to a steady state slower. Instead, some inhomogeneous, but close to the real distribution should be implemented. If there is a result from a previous run for similar conditions, it is better if this result is accepted as an initial guess. Although, asymptotically in time, the same steady state should be achieved, regardless of the initial condition of the system, a good initial guess may significantly shorten the time necessary for that. In each time step, the density is calculated from the particles coordinates and assigned to the computational grid nodes. This is done by the so-called area weighting. The next step is to solve the Poisson's equation on the grid. An efficient method to do so in (r,z) geometry, i.e. no θ dependence, is the cyclic reduction method [17]. Next, the Lorentz force is calculated on the grid and linearly interpolated to each particle. After that, the particles are moved and checked for collisions with the neutrals or with the walls. The accounted collisions are electron impact ionization and excitation of argon atoms from the ground state, elastic scattering of electrons, elastic and charge transfer collisions between argon ions and atoms and ion impact ionization. Due to the low degree of ionization Coulomb collisions are disregarded. Before the next time step, if new particles are created by ionization or ejection from the walls, they are added to and the lost through the walls particles are removed from the database. The ion trajectories are calculated once per every ten electron time steps. This is known as electron sub cycling [18] and leads to significant speeding of the procedure. The argumentation is that ions being roughly 8000 times heavier than electrons hardly change their coordinates in one electron time step. The procedure is stopped when the change of the characteristic parameters do not exceed the desired preset accuracy during few hundred time steps. In this simulation it was stopped after the anode and cathode currents became equal and their value differed less than 1 percent in 10000 time steps. The chart flow of the method is shown in Fig. 2.

The knowledge of the coordinates and velocity of every particle in each time step means that all macro characteristics of the entire discharge are known. In contrast to the fluid models electron and ion energy distribution functions and mean temperatures are self consistently obtained, and no initial assumption was necessary. The typical results of a PIC/MCC simulation include, among others, electron and ion density, mean energy, velocity and flux distribution, electric potential and field, EEDF and IEDF, ionization and excitation rates, angular and energy distribution of the ions at the cathode, energy loss through the walls. Some of them are presented below for conditions: pressure 3 mtorr, applied cathode voltage -270 V, maximal **B** 330 G and secondary electron emission coefficient γ = 0.1. For the ions absorption is assumed at all electrodes. At the cathode, electrons are reflected with probability 0.5. The walls are grounded and act as an anode.

Presented results describe in a self-consistent manner the entire discharge. They are in principle agreement with other simulations at similar conditions, as well as, with measured data. The EEPF shows the presence of a significant group of electrons with energies up to the discharge voltage. The sheath thickness above the racetrack is found to be 1.9 mm. The bulk potential has an axial variation from -55 V to + 5 V. This agrees with the measurements in [10], where the range was reported to be between -35V and +5V, but the more negative value was taken at 1 cm from the cathode. The radial electric field has significant values in the sheath and presheath. This explains the expansion of the angular ion distribution at the cathode towards bigger angles.

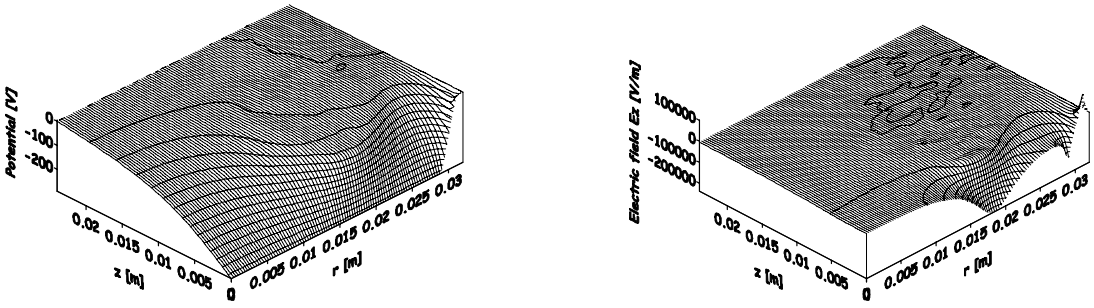

Fig. 3 Electric potential (left) and axial component of the electric field (right)

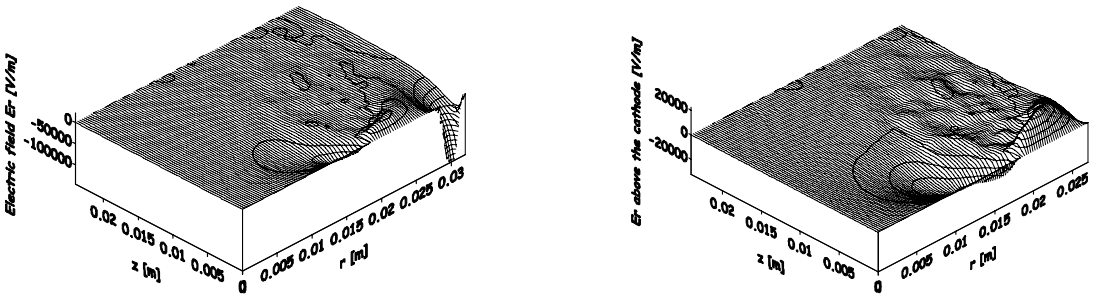

Fig. 4 Radial component of the electric field in the entire discharge (left) and above the cathode (right)

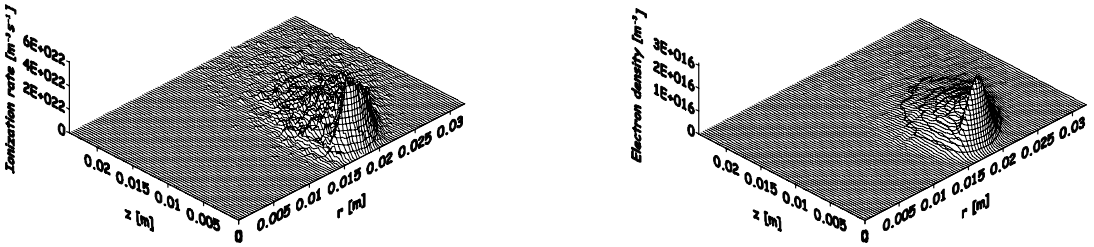

Fig. 5 Ionization rate (left) and electron density (right)

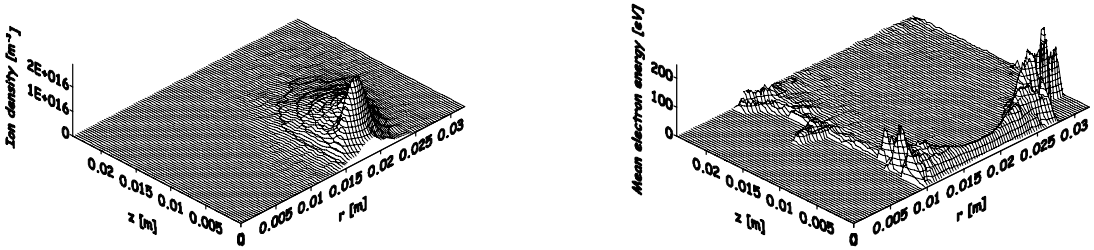

Fig. 6 Ion density (left) and mean electron energy distribution (right)

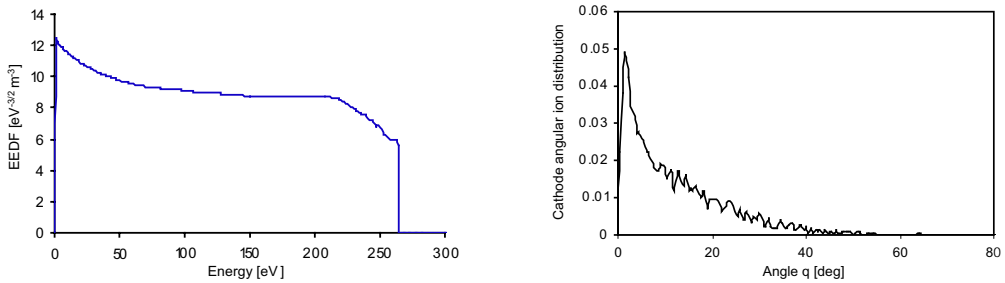

Fig. 7 Electron energy prabability function (EEPF, left)

4 Conclusion

Two methods - hybrid Fluid/Monte Carlo and PIC/MCC for numerical modeling of a DC planar magnetron were explained in detail and typical results from them shown. Both methods capture the main picture in magnetized discharges. However, the first method has limited application for not too high values of **B**/n. This is a limitation of the classical description of the electron transport across **B** lines. We didn't perform a detailed study to determine the critical value of **B**/n, up to where the model holds, but can qualitatively say that for pressures above 10 mtorr and $\mathbf{B}$ <150 G, reasonable results could be yielded at attractive computational cost. When the operational conditions are beyond this range a particle approach is needed. This is also necessary, when EEDF and IEDF are desired as results. The PIC/MCC method is the most powerful tool to tackle the problem with the full description of the planar magnetrons at all operational conditions. The price for that is the very long computational time.

References

[1] J.W. Bradley, G. Lister, Plasma Sources Sci. Technol. **6**, 524 (1997).
[2] L. Pekker, Plasma Sources Sci. Technol. **4**, 31 (1995).
[3] J.W. Bradley, Plasma Sources Sci. Technol. **7**, 572 (1998).
[4] N.F. Cramer, J. Phys. D: Appl. Phys. **30**, 2573 (1997).
[5] T.A. van der Straaten, N.F. Cramer, I.S. Falconer, E.W. James, J. Phys. D: Appl. Phys. **31** 177, 191 (1998).
[6] K. Nanbu, S. Segawa, S. Kondo, Vacuum **47**, 1013 (1996).
[7] S. Kondo, K. Nanbu, J. Phys. D: Appl. Phys. **32**, 1142 (1999).
[8] E. Shidoji, H. Ohtake, Nakano, T. Makabe, Jpn. J. Appl. Phys. **38**, 2131 (1999).
[9] K. Ness, T. Makabe, Phys. Rev. E, 4083 (2000).
[10] J.W. Bradley, S. Thompson, Y. Aranda Gonzalvo, Plasma Sources Sci. Technol. **10**, 490 (2001)
[11] C.K. Birdsall, A.B. Langdon, Plasma Physics via Computer Simulations (New York: McGraw-Hill) (1985).
[12] V. Vahedi, M. Surendra, Comp. Phys. Comm. **87**, 179 (1995).
[13] K. Nanbu, Jpn. J. Appl. Phys. **33**, 4752 (1994).
[14] K. Nanbu, S. Uchida, Rarefied Gas Dynamics 19, vol.1 (Oxford: Oxford University Press) p.602 (1995).
[15] A. Okhrimovskyy, A. Bogaerts, R. Gijbels, Phys. Rev. E **65**, 037402 (2002).
[16] S. Patankar, Numerical Heat transfer and Fluid Flow, Hemisphere Publishing Corp. (1980).
[17] R.W. Hockney, J.W. Eastwood, Computer Simulations Using Particles (New York: Adam Hilger) (1988).
[18] E. Kawamura, C.K. Birdsall, V. Vahedi, 2000 Plasma Sources Sci. Technol. **9**, 413 (2000).